Optical Engineering

OpticalEngineering.SPIEDigitalLibrary.org

Optimal design of linear tapered double S-shaped arrayed waveguide grating for broad channel spacing on silicon-on-insulator

Nurjuliana Juhari
P. Susthitha Menon
Abang Annuar Ehsan
Sahbudin Shaari

SPIE.

Optimal design of linear tapered double S-shaped arrayed waveguide grating for broad channel spacing on silicon-on-insulator

Nurjuliana Juhari, P. Susthitha Menon,* Abang Annuar Ehsan, and Sahbudin Shaari
Universiti Kebangsaan Malaysia (UKM), Institute of Microengineering and Nanoelectronics, 43600 Bangi, Selangor, Malaysia

Abstract. A linear tapered double S-shaped arrayed waveguide grating (AWG) was designed as an alternative to a U-shaped AWG, and a complete transmission spectrum for 18 channels of coarse wavelength-division multiplexing (CWDM) was demonstrated. The silicon-on-insulator based AWG with a rib waveguide structure with a broad channel spacing of 20 nm was designed to serve as a multiplexer/demultiplexer. A beam propagation method modeling simulation under transverse electric mode polarization over a free spectrum range of 700 nm was used for the design process. The geometrical dimensions of the AWG rib structure were optimized to achieve the lowest reported insertion loss of 1.07 dB and adjacent crosstalk of −38.83 dB. The influence of different etching depths on the top Si layer of the AWG for a constant core width of 0.6 μm as well as birefringence effects were also investigated. A transmission spectrum response at the output port close to the standard CWDM wavelength grid range of 1271 to 1611 nm with an average channel spacing of 2485 GHz was obtained.
 [DOI: 10.1117/1.OE.53.8.087110]

Keywords: arrayed waveguide grating; coarse wavelength-division multiplexing; broad channel spacing; crosstalk; rib waveguide on silicon-on-insulator; birefringence.

Paper 140766 received May 12, 2014; revised manuscript received Aug. 1, 2014; accepted for publication Aug. 5, 2014; published online Aug. 28, 2014.

1 Introduction

Silicon-on-insulator (SOI) has become a popular choice of material in recent years because of its potential for use in the photonics components manufacturing industry, which uses a monolithic or hybrid integration assembly. Arrayed waveguide gratings (AWG)-based silicon waveguide structures functioning as multiplexers/demultiplexers (mux/demux) are being widely employed in wavelength-division multiplexing (WDM) systems. There are several advantages in using SOI as a platform for photonics integration, such as low manufacturing costs due to the use of existing complementary metal oxide semiconductor fabrication technology,[1] compact devices, and high confinement of the optical mode.[2] Further, silicon has a high index contrast (Δn) and is transparent at infrared wavelengths, making it suitable for optical communication applications. By using these features of SOI materials, we designed and analyzed an SOI-based AWG mux/demux capable of splitting or combining the multiple signals in a single fiber utilized in coarse wavelength-division multiplexing (CWDM) systems.

In this work, we optimized the geometrical rib waveguide structure and characterized the ideal parameters of a linear tapered double S-shaped AWG on an SOI platform to mitigate insertion loss (IL) and adjacent crosstalk (XT) in an 18-channel CWDM device with a channel spacing of 20 nm. The investigations were carried out by selecting the dimensions of the rib waveguide, which allows a single-mode condition where the ratio of the slab height (h) to the thickness of the top silicon (Si) guiding layer (H) or h/H was in the range of 0.7 to 0.85. For each value of h/H, the core width was also varied between 0.5 and 1.2 μm. The range of H values is specific to the 18-channel AWG with broad channel spacings. In previous works, we have achieved IL of <7 dB[3] and <4.03 dB,[4] respectively. The IL was further reduced to 3 to 6 dB when the commonly used linear tapered waveguide was used in the AWGs.

Due to imperfections in the AWG fabrication process, such as in lithography or in etching, random phase errors of the arrayed waveguides may occur and affect the adjacent XT and IL values. Okamoto[5] reports that the thickness fluctuation of the top Si layer in the SOI wafer was in the range of 0.5 to 1.0 nm and affected the adjacent XT by −20 dB. Meanwhile, a photo-mask resolution of 25 nm causes the adjacent XT to drop to < -30 dB.[6] For a shallow-etched Si nanowire AWG with varied etch depths, the deviation in the core width is in the range of 3 to 8 nm.[7] Owing to small variations of ∼20 nm in the etching profile, one linear AWG device with the same core width and different etch depths were carried out to identify the adjacent XT and IL behavior. Using the same size of core width, the effect of birefringence was also analyzed in order to compensate the wavelength shift. Besides the reduction in IL and adjacent XT, we also aim to obtain an AWG with a channel central wavelength that complies with the CWDM grid and with a channel spacing tolerance of ±5 nm.

2 AWG Design Parameter

Three different sets of input parameters were considered in the process of designing the AWG device.[8]

1. Technological parameter: Here we chose SOI as the substrate to design the AWGs, where the refractive

*Address all correspondence to: P. Susthitha Menon, E-mail: susi@eng.ukm.my

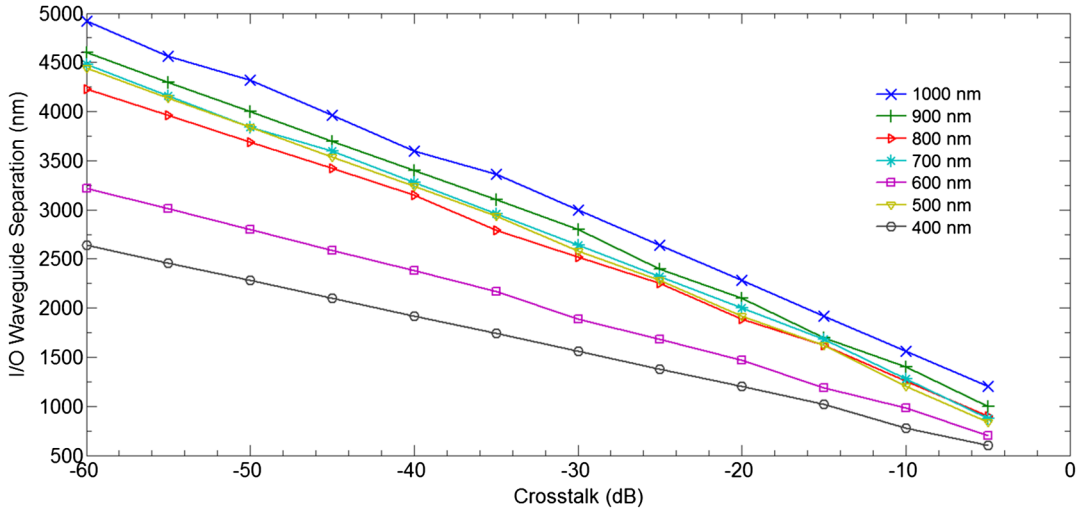

Fig. 1 Theoretical values of adjacent crosstalk with respect to the input/output (I/O) waveguide separation width (D) for different thicknesses of the top Si guiding layer (H). Values of D were chosen so that the adjacent crosstalk (XT) is better than –35 dB in the coarse wavelength-division multiplexing (CWDM) transmission spectrum.

index of Si is $n_{Si} = 3.5$ and the lower cladding layer is SiO_2, where $n_{SiO_2} = 1.5$. A rib waveguide structure is proposed where the dimensions of the waveguide cross-section are explained in Sec. 3.

2. AWG type parameter: The transverse electric (TE) polarization mode with 18 output channels was selected. Since the CWDM spectrum ranges from 1271 to 1611 nm, the channel central wavelength of the AWG is set to be at 1431 nm and the channel spacing is ~2500 GHz.
3. Transmission parameters: The AWG design is targeted to exhibit an adjacent XT of < -35 dB and IL nonuniformity of <1 dB. The minimum separation between the centers of two neighboring input/output (I/O) waveguides (D) and the arrayed waveguides (d) can be determined using modal fields and is predefined by the maximum adjacent XT level, $XT_{MAX} = 10\log(P_{over})$, where P_{over} is the overlap integral equation. The nonuniformity Lu $\approx 8.7\theta_{max}/\theta_0$, where θ_0 is the width of the equivalent Gaussian far field, was also determined. Figure 1 shows the theoretical calculation of the adjacent XT where suitable values of the I/O waveguide separation width (D) can be selected for a given top Si guiding layer thickness (H) while maintaining the adjacent XT to be > -35 dB. Figure 2 shows that the theoretical nonuniformity is maintained <1 dB for all the different values of H.

3 Optimization on Dimension of Rib Waveguide

The cross-section of the rib waveguide structure was determined using Eqs. (1) and (2) (Ref. 9) for a single-mode condition, where W, H, and h are the core width, thickness of top Si layer, and slab height, respectively.

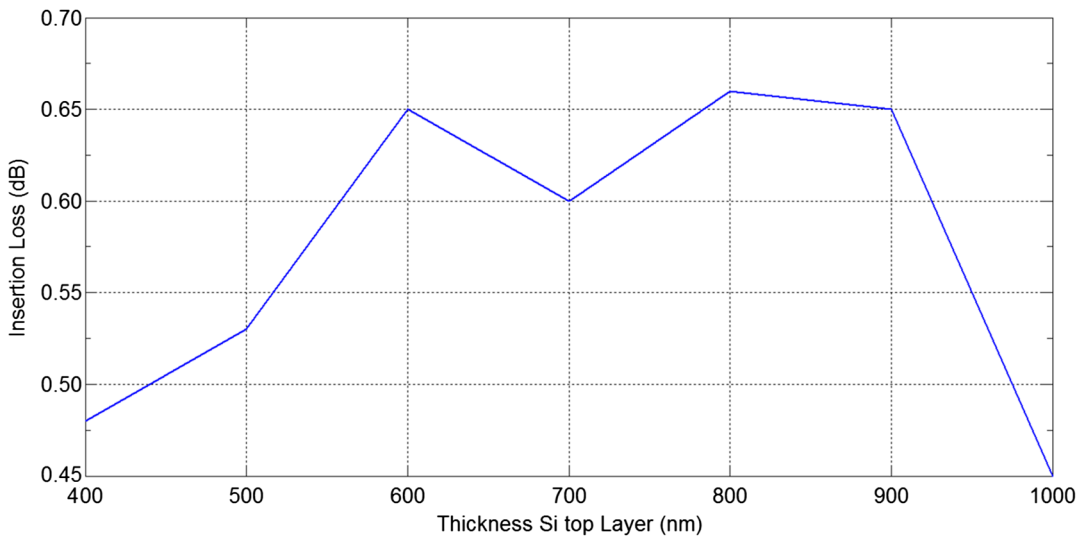

Fig. 2 Theoretical values of nonuniformity are <1 dB for different thicknesses of the top Si guiding layer (H).

$$\frac{W}{H} = 0.3 + \frac{\frac{h}{H}}{\sqrt{1 - \left(\frac{h}{H}\right)^2}}, \quad (1)$$

$$\frac{h}{H} \geq 0.5. \quad (2)$$

Then, we confirmed that this rib waveguide provided single-mode propagation by simulating the structure using the OptiBPM simulator performing under the quasi-TE mode solver. To achieve 18-channels' transmission with a 20 nm channel spacing using a double S-shaped AWG design, the thickness of the top Si layer should be in the range of 0.4 to 1.0 μm. We found that if the thickness was <0.4 μm, an 18-channel transmission spectrum could not be achieved. Moreover, if the thickness exceeded 1.0 μm, the larger bending radius with a high loss and large device footprint was produced. Thus, the minimum and maximum thicknesses for the top Si layer were set to 0.4 and 1.0 μm, respectively. We used WDM-Phasar software to optimize the value of the ratio h/H. Values in the range of 0.75 to 0.8 resulted in the best performance for simulations under single-mode propagation. The simulation was run using the optimized value of the ratio h/H along with different values of the top Si layer thickness. Figure 3

Si layer (H)			
Top Silicon layer thickness (H), μm	Core width (W), μm	Slab height (h), μm	Single mode profile under TE mode
0.4	0.5	0.3	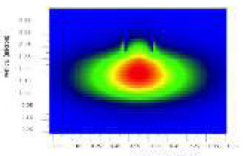
0.5	0.6	0.40	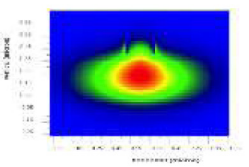
0.6	0.7	0.45	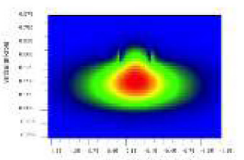
0.7	0.8	0.55	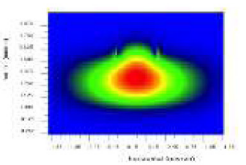
0.8	0.9	0.62	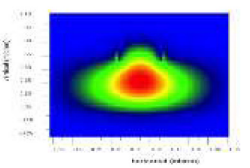
0.9	1.0	0.70	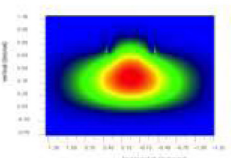
1.0	1.2	0.80	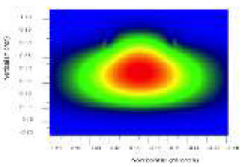

Fig. 3 The single-mode profile in the cross section of the arrayed waveguide grating rib waveguide for different thicknesses of the top Si layer (H).

displays the cross-section and profile pattern for single-mode propagation in the rib waveguide structure operating in the TE mode with a 1431 nm AWG channel central wavelength for the top Si layer thickness in the range of 0.4 to 1.0 μm.

4 Optimization of AWG Design Layout

Figure 4 shows a schematic of the SOI-based AWG computer aided design (CAD) layout with a rib waveguide structure, which was designed using the WDM-Phasar simulator, for 18 channels of the CWDM transmission spectrum. The architecture of the AWG device consists of 18 I/O ports, 72 arrayed waveguides with constant optical path length increments (ΔL) between neighboring waveguides, and two symmetrical free propagation regions (FPR). The layout pattern is the same for all thicknesses of the top Si layer, but other parameters, such as the modal index, ΔL, FPR, free spectral region, and nonuniformity, were different. Four geometrical parameters of the AWG structure that must be calculated in order to get the correct AWG demultiplexing properties are the length of the FPR (or focus length, f), the minimum waveguide separation width between two neighboring waveguides in the phased array (d) and at the I/O waveguides (D), as well as the constant optical path length increment (ΔL). For example, the FPR for a 1.0-μm-thick top Si layer was 794.019 μm long on both sides of the AWG. Using the equation $\Delta L = \lambda_0 \cdot m/n_c$ for the same thickness of the top Si layer, ΔL is 0.823 μm when $m = 2$, $\lambda_0 = 1.431$ μm (2930 GHz), and $n_c = 3.4763235$ were chosen. Three parameters play a critical role in optimizing the AWG device to achieve a low loss, smaller footprint, and good performance in terms of adjacent XT and IL. These parameters are the bending radius, the total number of arrayed waveguides, and the initial length increment. The initial length increment is a special parameter in the AWG-Phasar tool that allows change in the bending of the waveguides in the phased array and it is defined as the difference between the distance span of the path and the length along the path. With an increase in the number of arrayed waveguides, the AWG experienced a high optical loss, especially in the arrayed waveguide region, due to the large S-bending radius. On the other hand, when the number of arrayed waveguides increased, the possibility of coherent interference, in which identical wavelengths with the same phase order pass through each i'th arrayed waveguide, was increased. Therefore, for this model 72 arrayed waveguides were used. The initial length increment depends on the thickness of the top Si layer. The maximum (1.0 μm) and minimum (0.4 μm) thicknesses of the top Si layer results in initial length increments of 1500 and 3200 μm, respectively. Furthermore, the total device size and bending radius were different for different thicknesses of the top Si layer. For example, for a 1.2 μm core width with a 1.0 μm top Si layer thickness, the first arrayed waveguide produced a total bending radius of 829.404 μm with a total loss of 0.097 dB over a total AWG device length of 7466 μm, while the last arrayed waveguide produced a total bending radius of 1025.628 μm with a 0.065 dB loss over a total AWG device length of 7524 μm. In accordance with Pearson et al.,[10] the bending radius obtained from this simulation is within the fundamental mode regime. Moreover, the minimum bending radius reported for high-index contrast materials is <2 mm,[11] and this indicates that our design results in an improved bending radius. For the example mentioned above, the total size of the AWG on chip is 48 mm × 9 mm.

Existing AWG devices use a U-shaped pattern.[12,13] However, for broad channel spacing (20 nm), where ΔL is very small, the WDM-Phasar simulator is incapable of connecting all the arrayed waveguides for an AWG with a U-shaped pattern. Therefore, the double S-shaped pattern was used for the AWG, where the higher losses incurred in this pattern are compensated with the usage of a high-index contrast material. Optical light beams couple if the distance between adjacent waveguides in the arrayed waveguide region is <3 μm. AWGs with an S-shaped pattern have also been used in other practical devices,[14] such as in broadband InP AWGs. However, the arrayed waveguide region was different when an antisymmetric S-shaped pattern was used. In this work, the commonly used linear tapered waveguide design was also used in the FPR for the incoming and outgoing waveguides to reduce the IL and adjacent XT as shown in Fig. 5. The diffraction loss is influenced by the value of the minimum arrayed waveguide separation, d. For the linear tapered region, the entrance width W_1, exit width W_0, tapered length L_{tap}, and tapering angle δ are related as $W_0 = W_1 - 2L_{tap} \tan \delta$.[15] This relationship is illustrated in Fig. 5, where Z is the direction of the propagation of light. Table 1 lists the values of each parameter for different thicknesses of the top Si layer.

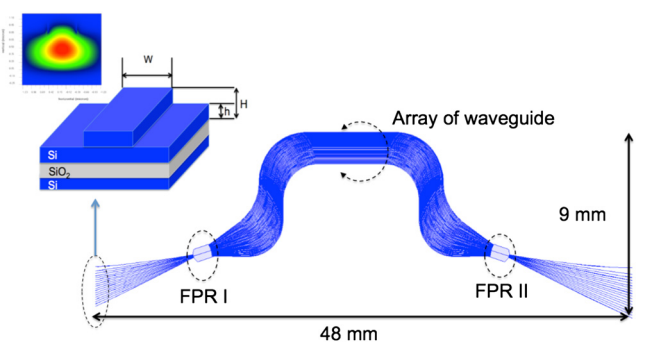

Fig. 4 Schematic of a double S-shaped arrayed waveguide grating (AWG) using a rib-waveguide structure. The left and right arms of the array of waveguides result in a symmetric value of bending radius and single-mode propagation under TE polarization is launched at the input waveguide.

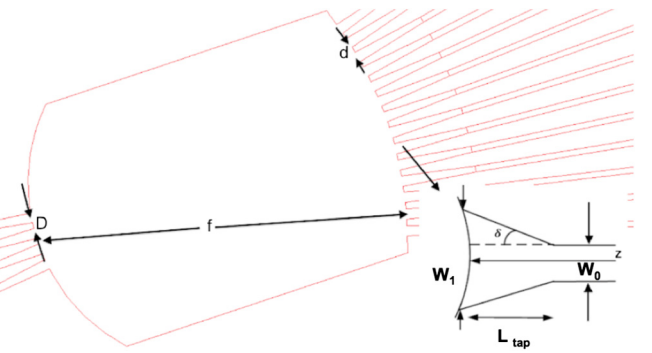

Fig. 5 Schematic of free propagation region showing the position of linear tapered, minimum input/output waveguide separation (D), focus length (f), minimum arrayed waveguide separation (d), entrance tapered width (W_1), and exit tapered width (W_0).

Table 1 Parameter for tapered waveguide at free propagation region (FPR).

Top Si layer thickness, H (μm)	Entrance tapered width, W_1 (μm)	Exit tapered width, W_0 (μm)	Tapered length, L_{tap} (μm)
0.4	2.02	0.5	47.08
0.5	2.81	0.6	91.75
0.6	1.85	0.7	60.42
0.7	3.05	0.8	108.32
0.8	2.95	0.9	105.48
0.9	3.3	1.0	128.89
1.0	3.0	1.2	158.8

5 Simulation Results and Discussion

Figures 6(a) and 6(b) plot the IL and adjacent XT as functions of the channel number for different values of the top Si layer thickness between 0.4 and 1.0 μm, over 18 channels ranging from 1271 to 1611 nm. These data were extracted from the original transmission spectrum as shown in Fig. 7. The lowest IL was observed at the central channel (channel number 9 with a wavelength of 1431.6 nm), while the highest IL was observed in the peripheral channels which are far apart from the central channel. This distribution pattern occurs because the far-field intensity of each individual waveguide is reduced with the distance away from the origin of the central wavelength. The nonuniformity between the central channel and the peripheral channels is ~1 to 5 dB for different values of the top Si layer thickness. This value is high when compared with the theoretical data presented in Fig. 2 where the IL was <1 dB. When the thickness of the top Si layer was decreased, the IL increased in the range of 1.0 to 3.0 dB at the central wavelength. This is because the core width (W) decreases with a decrease in the top Si guiding layer thickness, and when W becomes smaller than the minimum arrayed waveguide separation width (d), a high diffraction loss is observed at the first FPR. To overcome this issue, a standard tapered design was included at both FPRs, which is a common method used to reduce IL.[16] As shown in Fig. 6(b), the usage of a tapered design produced similar adjacent XT values of −13.5 dB for top Si layer thicknesses of 0.4 and 1.0 μm for channel number 9. The lowest adjacent XT of −38.83 dB was observed in the same channel for a top Si guiding layer thickness of 0.7 μm. This value exhibits the best result for the adjacent XT. Adjacent XT values of −35.45, −26.28, −19.69, and −15.92 dB were obtained for the top Si layer thicknesses of 0.9, 0.8, 0.5, and 0.6 μm, respectively. For the top Si guiding layer of 1.0 μm, the adjacent XT exhibits a large value of −12.67 dB due to the effect of side lobes. Note that the adjacent XT can be reduced by decreasing the value of d and increasing the value of D.[17] However, our proposed design uses the same values for both d and D in order to maintain the adjacent XT to be > -35 dB. Besides, the values of d and D can be adjusted depending on the design parameters. The plot in the graph

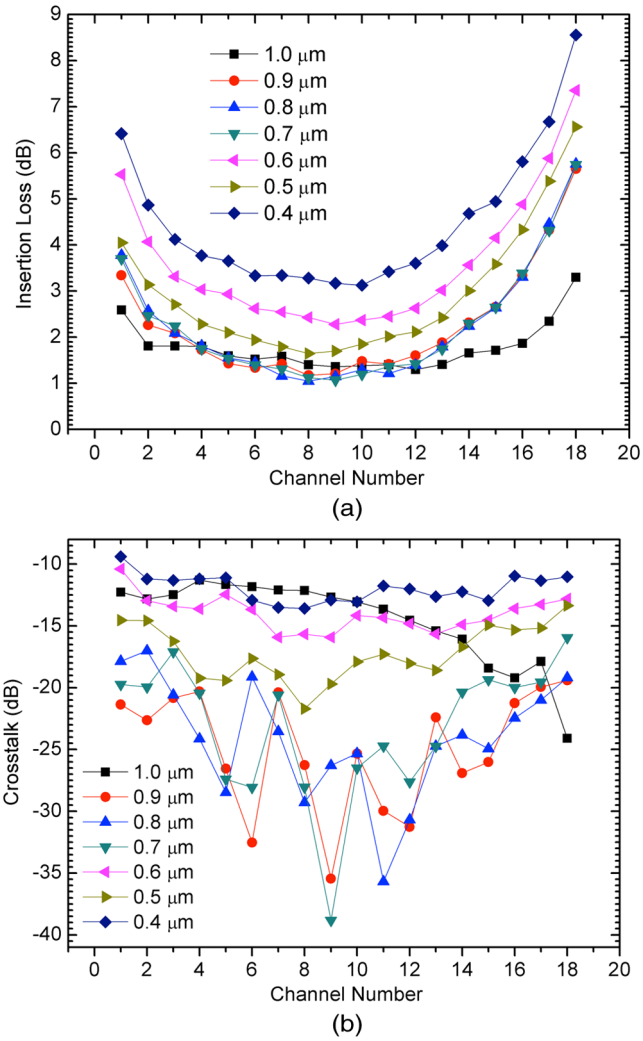

Fig. 6 Simulation results of (a) insertion loss and (b) adjacent XT for different thicknesses of top silicon layer for all 18 channels of the CWDM AWG demultiplexer.

shows that no direct relationship exists between the adjacent XT and the thickness of the top Si layer. However, the AWG design results in values comparable with those produced by existing practical devices that have different channel spacing but are fabricated using the same material (SOI).[13,17,18] The lowest IL, with a higher adjacent XT, was obtained for an AWG design with a top Si layer thickness of 1.0 μm and a core width of 1.2 μm. The complete transmission spectrum of an 18-channel AWG is shown in Fig. 7. It has a central wavelength close to that of the CWDM wavelength grid with an average channel spacing of ~2500 GHz (19.9 nm). For example, a central wavelength of 1431.6 ± 5 nm is obtained at the center of the spectrum. Furthermore, for a top Si guiding layer thickness of 1.0 μm, the relationship among the entrance tapered waveguide width (W_1) and the adjacent XT as well as the IL values for a complete CWDM channel was investigated. When the taper width was increased, the adjacent XT is predicted to be higher due to a higher evanescent coupling between the output waveguide with reduced IL. Thus, as predicted, when the maximum entrance tapered waveguide width was increased from 2.2 to 3 μm, the IL is reduced but the adjacent XT is increased. For example, in

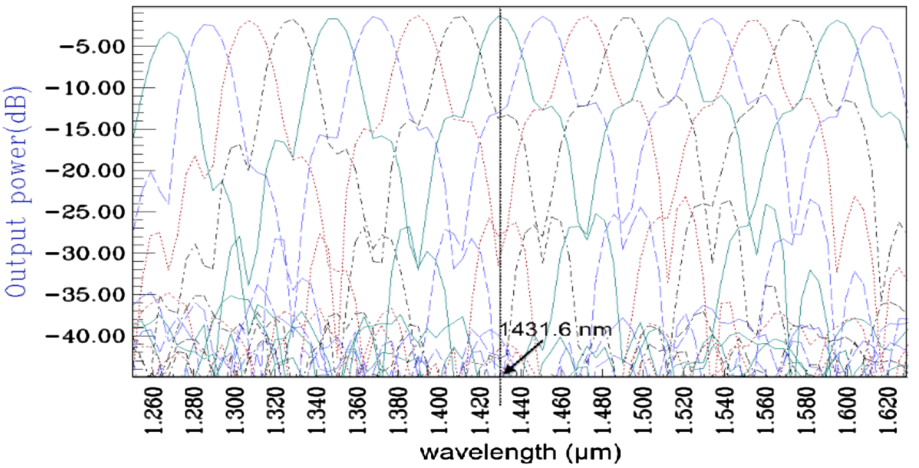

Fig. 7 Simulation results for transmission spectrum of 18-channel AWG demultiplexer obtained from a 1.0-μm-thick top silicon layer with core width of 1.2 μm.

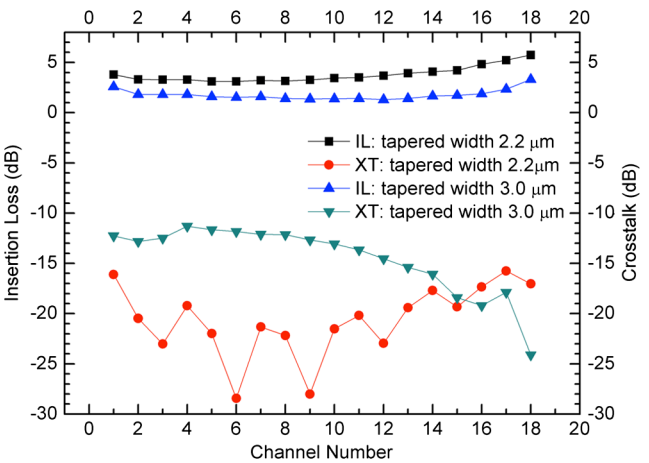

Fig. 8 The comparative results of insertion loss (IL) and adjacent XT as a function of channel spacing/number when the entrance tapered waveguide width (W_1) is increased from 2.2 to 3.0 μm for a top Si layer thickness of 1.0 μm.

channel number 9, the IL is reduced to 2 dB and the XT increased to 16 dB, respectively, as illustrated in Fig. 8.

When the thickness of the top Si guiding layer of the CWDM AWG was varied, no significant relationship was observed for the insertion loss and the adjacent XT as many AWG design parameters were also simultaneously varied. Therefore, in order to investigate the effect of imperfections in the CWDM AWG fabrication processes, such as in lithography or in etching, the top Si guiding layer thickness (H) was varied by ~20 nm while maintaining the core width (W) at 0.6 μm and the slab height (h) at 0.4 μm. The top Si guiding layer thickness (H) was varied from 0.5, 0.52, 0.54, and 0.56 μm, which corresponds to etching depths of 0.1, 0.12, 0.14, and 0.16 μm, respectively. When compared to the AWG design parameters listed in Table 1, a small modification was made to the tapered length, L_{tap}, and the entrance tapered width (W_1) for a 0.5 μm top Si guiding layer as tabulated in Table 2, where L_{tap} was expanded from 91.75 to 103.22 μm, while W_1 was changed from 2.81 to 3.1 μm. These values were consistently used for all the subsequent AWG designs in order to effectively evaluate the effect of imperfections in the CWDM AWG fabrication processes. A summary of the AWG design parameters for the waveguide cross-section values, entrance tapered waveguide width, exit tapered waveguide width, and the tapered length is tabulated in Table 2. Other AWG design parameters are the same as discussed in Sec. 2. Figure 9 presents the IL and adjacent XT as a function of the channel spacing/number for incremental etch depths from 0.1 to 0.16 μm, which was extracted from the 18-channel CWDM transmission spectrum as illustrated in Fig. 10. At the central waveguide channel, for etch depths of 0.1, 0.12, 0.14, and 0.16 μm, IL values increased from 1.36, 1.72, and 1.97 dB to 2.59 dB, respectively. Meanwhile, the adjacent XT for the same central waveguide also decreased with values of −19.87, −17.37, −15.51, and −14.95 dB, respectively. Therefore, when the etch depth is increased, the IL and

Table 2 New parameter values for cross-section of rib waveguide and tapered waveguide at FPR.

Top Si layer thickness, H (μm)	Core width, W (μm)	Slab height, h (μm)	Entrance tapered width, W_1 (μm)	Exit tapered width, W_0 (μm)	Tapered length, L_{tap} (μm)
0.50	0.60	0.40	3.1	0.60	103.22
0.52	0.60	0.40	2.7	0.60	103.22
0.54	0.60	0.40	2.4	0.60	103.22
0.56	0.60	0.40	2.2	0.60	103.22

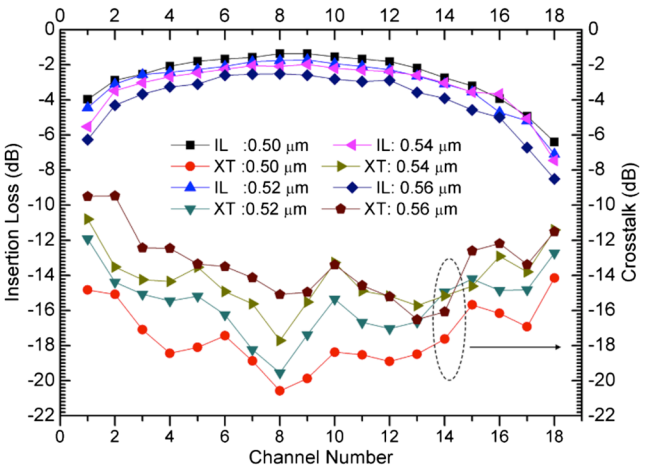

Fig. 9 The comparative results of IL and adjacent XT as a function of channel spacing/number when the etching depth is increased from 0.1 to 0.16 μm with a constant core width of 0.60 μm for TE mode polarization.

adjacent XT decreased. Therefore, the best design parameter combination for a CWDM SOI-based AWG in order to obtain a low insertion loss and adjacent XT is reached the top Si thickness is 0.5 μm for each 0.1 μm of depth and core width of 0.6 μm.

Using the best design parameter combination for the CWDM AWG, the effect of birefringence was analyzed in order to evaluate the polarization-dependent wavelength shift (PDλ), which is given by $\mathrm{PD}\lambda = \lambda(n_{\mathrm{TE}} - n_{\mathrm{TM}})/n$, where n_{TE} is the refractive index in the TE mode and n_{TM} is the refractive index in the transverse magnetic (TM) mode. Figure 11 shows the calculated effective index and PDλ as a function of the Si etch depth for the CWDM AWG. When the etch depth is gradually decreased from 0.16 to 0.1μm, the birefringence ($n_{\mathrm{TE}} - n_{\mathrm{TM}}$) was completely reduced and almost nullified for an etch depth of 0.1 μm with a core width of 0.6 μm. As for the calculated PDλ, a core width of 0.6 μm and Si etch depth of 0.1 μm causes the PDλ to be <0.0005 nm. For confirmation purposes, the calculated values were compared with a simulated CWDM AWG with an Si etch depth of 0.1 μm and a core width of 0.6 μm. The spectral response at the central wavelength channel of 1431 μm for both polarization modes was then compared and illustrated in Fig. 12,

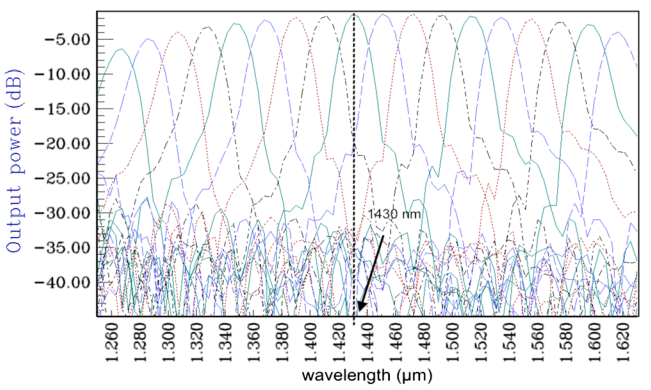

Fig. 10 Simulation results for transmission spectrum of 18-channel AWG demultiplexer obtained from a 0.5-μm-thick top silicon layer with core width of 0.6 μm.

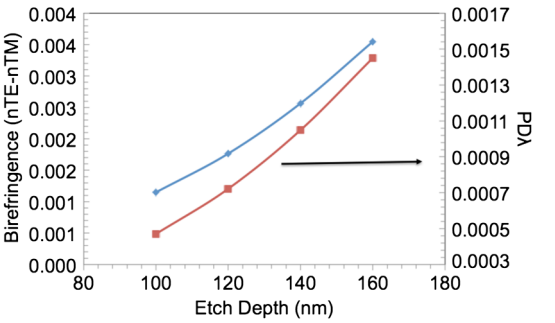

Fig. 11 Calculated birefringence ($n_{\mathrm{TE}} - n_{\mathrm{TM}}$) and polarization-dependent wavelength shift (PDλ) for a rib waveguide silicon-on-insulator-based CWDM AWG when the etching depth is varied from 0.1 to 0.16 μm with a constant core width of 0.6 μm.

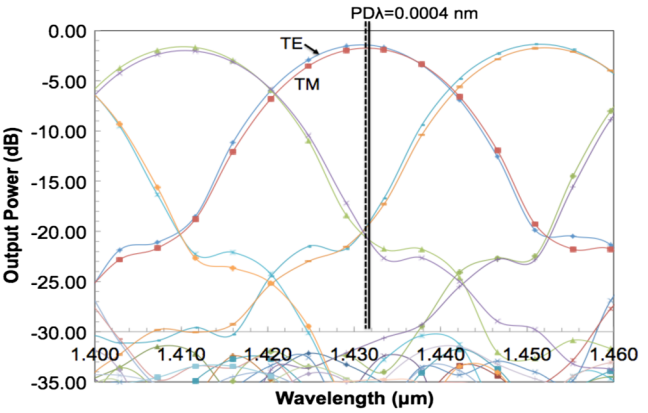

Fig. 12 Simulated spectral response of 18-channel CWDM AWG demultiplexer with a core width of 0.6 μm and ratio $h/H = 0.80$ exhibiting an almost nullified PDλ, where both the TM and TE spectrums tend to overlap at the central wavelength channel of 1431 nm.

where the value of the PDλ is ~0.0004 nm and agrees with the calculated value.

6 Conclusion

We successfully developed an SOI-based linear tapered double S-shaped rib-AWG demultiplexer using beam propagation method under TE mode polarization with average channel spacing of 2485 GHz. We obtained the lowest IL and adjacent XT after inserting tapered regions at the I/O waveguide and arrayed arms in the FPR, for a top Si layer thickness of 0.7 μm with a core width of 0.8 μm. Fabrication intolerances causing an increment in etch depths of the top Si layer of the AWG rib waveguide by 20 nm deteriorated the IL, adjacent XT, and birefringence. Moreover, the complete transmission spectrum obtained using a 1.431 μm central wavelength launch was close to the standard CWDM wavelength grid for which this device successfully performed as a demultiplexer.

Acknowledgments

This work has been filed for patent by Universiti Kebangsaan Malaysia (UKM) under filing No. UKM3.2.29/108/2/741 and is supported by the Malaysian Ministry of Education under research grant FRGS/2/2013/SG02/UKM/02/4.

References

1. X. Chen, C. Li, and H. K. Tsang, "Device engineering for silicon photonics," *NPG Asia Mater.* **3**(1), 34–40 (2011).
2. G. Roelkens et al., "Grating-based optical fiber interfaces for silicon-on-insulator photonic integrated circuits," *IEEE J. Sel. Topics Quantum Electron.* **17**(3), 571–580 (2011).
3. N. Juhari et al., "Optical loss analysis in 13-channel SOI-based AWG for CWDM network," *J. Nonlinear Opt. Phys. Mater.* **23**(1), 1450008 (2014).
4. N. Juhari, P. S. Menon, and A. A. Ehsan, "12-channel tapered SOI-based AWG for CWDM system," in *Proc. IEEE*, pp. 230–233, IEEE, Malaysia (2013).
5. K. Okamoto, "Progress and technical challenge for planar waveguide devices: silica and silicon waveguides," *Laser Photon. Rev.* **6**(1), 14–23 (2012).
6. C. D. Lee et al., "The role of photomask resolution on the performance of arrayed-waveguide grating devices," *J. Lightwave Technol.* **19**(11), 1726–1733 (2001).
7. D. K. Kim et al., "Crosstalk reduction in a shallow-etched silicon nanowire AWG," *IEEE Photon. Technol. Lett.* **20**(19), 1615–1617 (2008).
8. D. Seyringer and M. Bielik, "AWG-parameters: new software tool to design arrayed waveguide gratings," *Proc. SPIE* **8627**, 862716 (2012).
9. O. Powell, "Single-mode condition for silicon rib waveguides," *J. Lightwave Technol.* **20**(10), 1851–1855 (2002).
10. M. R. T. Pearson et al., "Arrayed waveguide grating demultiplexers in silicon-on-insulator," *Proc. SPIE* **3953**, 11–18 (2000).
11. K. Okamoto, *Fundamental of Optical Waveguide*, 2nd ed., Elsevier Academic Press, San Diego, California (2005).
12. D. Seyringer et al., "Design, simulation, evaluation, and technological verification of arrayed waveguide gratings," *Opt. Eng.* **53**(7), 071803 (2014).
13. H. Li et al., "Practical fabrication and analysis of an optimized compact eight-channel silicon arrayed-waveguide grating," *Opt. Eng.* **52**(6), 064602 (2013).
14. K. Rausch et al., "Broadband arrayed waveguide gratings on InP," *Opt. Quantum Electron.* **39**(7), 611–622 (2007).
15. Y. Xu and H. Lin, "A concise design of 16×16 polymer AWG with low insertion loss and crosstalk," *Optik* **125**(3), 920–923 (2014).
16. P. Muñoz et al., "Modeling and design of arrayed waveguide gratings," *J. Lightwave Technol.* **20**(4), 661–674 (2002).
17. H. Li et al., "Optimal design of an ultrasmall SOI-based 1x8 flat-top AWG by using an MMI," *Sci. World J.* **2**, 1–6 (2013).
18. H. Li et al., "Design of 1x8 silicon nanowire arrayed waveguide grating for on-chip arrayed waveguide grating demodulation integration microsystem," *Opt. Eng.* **51**(12), 123001 (2012).

Nurjuliana Juhari obtained her BSc and MSc from the University of Malaya in the physics department in 2003 and 2007. She is currently pursuing her PhD degree at Photonics Technology Laboratory, Institute of Microengineering and Nanoelectronics (IMEN), Universiti Kebangsaan Malaysia (UKM). Her research interests include design, fabrication, and characterization of passive devices in submicron-level silicon-on-insulator-based arrayed waveguide grating, applied in a coarse wavelength-division multiplexing system.

P. Susthitha Menon received her BEng degree in electrical, electronics, and systems engineering from the National University of Malaysia (UKM) in 1999 and her MS degree in optoelectronics from UKM in 2005. She obtained her PhD degree with distinction in optoelectronics and nanophotonics from the IMEN, UKM in 2008. She is currently a senior research fellow at IMEN and her current research interests are in the field of nanophotonic optical waveguides, surface plasmon resonance, optoelectronics and optical fiber based sensors, which are all geared toward biosensing.

Abang Annuar Ehsan received his BE degree in electrical engineering from University of New South Wales, Australia, in 1996 and his MSc degree in microelectronics from UKM in 2002. He received his PhD degree in applied science from Universiti Teknologi MARA, Malaysia, in 2010 and his PhD in microengineering and manoelectronics from UKM in 2012. His research interests include plastic optical fiber devices, planar optical waveguides, optical design and modeling, and rapid manufacturing of optical devices.

Sahbudin Shaari received his MSc degree in quantum electronics from University of Essex and his PhD degree in microelectronics from University of Wales in 1980 and 1989. From 1978 to 2003, he was a lecturer with the Department of Electrical, Electronic and System Engineering, UKM. In 1982, he introduced optical fiber communications in the country. He became a full professor in microelectronics/photonics in 2002. In 2003, he joined IMEN, UKM, Malaysia, as the head of the Photonics and Nanophotonics Research Group. Currently, his research interest is in the field of silicon photonics.